PCCP

COMMUNICATION

A Bowknot-like RuO_2 quantum dots@V_2O_5 cathode with largely improved electrochemical performance†

Cite this: *Phys. Chem. Chem. Phys.*, 2014, **16**, 18680

Received 24th June 2014,
Accepted 23rd July 2014

DOI: 10.1039/c4cp02762k

www.rsc.org/pccp

Xiujuan Wei, Qinyou An, Qiulong Wei, Mengyu Yan, Xuanpeng Wang, Qidong Li, Pengfei Zhang, Bolun Wang and Liqiang Mai*

Bowknot-like RuO_2 quantum dots@V_2O_5 nanomaterials have been synthesized by a facile hydrothermal method followed by annealing treatment, which exhibit largely enhanced electrochemical performance. Especially, the RuO_2 quantum dots@V_2O_5 cathode delivers 160 mA h g^{-1} at 1000 mA g^{-1} after 100 cycles, which is much higher than 86 mA h g^{-1} of the pure V_2O_5 cathode.

Introduction

With the global energy and environmental problems becoming more and more severe, the development of environmentally friendly and efficient energy storage systems are urgently required.[1,2] Lithium-ion batteries (LIBs) play an important role as energy storage devices for use in portable electronic devices, electric vehicles and electric grid due to their high energy-density, high safety and environmentally benign nature.[3–7] Among the potential cathode materials, vanadium pentoxide (V_2O_5) is one of the most promising materials for LIBs owing to its low cost, high energy density, easy synthesis, as well as a relatively high theoretical capacity of 294 mA h g^{-1} in the voltage range of 4.0–2.0 V *vs.* Li^+/Li.[8–10] Nevertheless, V_2O_5 suffers from low diffusion coefficient of Li^+, poor electrical conductivities (10^{-5}–10^{-3} S cm^{-1}) and poor structural stability, which limit the development of vanadium pentoxide electrode materials in LIBs.[11–13]

In order to improve the electrochemical performances of V_2O_5 electrode materials, various nanostructures of V_2O_5 have been successfully synthesized, including nanowires,[14,15] nanobelts,[16–18] nanotubes[19] and nanosheets.[20] These nanostructures can shorten the diffusion distance of Li^+ and accommodate large volume change during the lithium intercalation and de-intercalation processes.[21–23] Significant investigations have been carried out to develop unique nanostructured materials.[24,25] For example, Shi *et al.* synthesized the LiV_3O_8 thin film with a mixed amorphous–nanocrystalline exhibiting high capacity and good capacity retention.[26] Besides, the transportation of electrons within the electrode also exerts a significant impact on the rate capability of LIBs. The resistance arises from the low electronic conductivity of the electrode materials. Thus, it is required to use V_2O_5 in conjunction with another nanostructured material possessing higher electronic conductivity.[27–30] For example, Chen *et al.* constructed the MWCNT–V_2O_5 core–shell sponge for high power density.[31] Zhang *et al.* fabricated carbon-coated V_2O_5 with high performance.[32] RuO_2 exhibits high electronic conductivity (2.5×10^4 S cm^{-1}), fast Li^+ permeation and stable reaction interface (high coulombic efficiency above 98%), which has been extensively studied by many researchers.[33–35] Maier and co-workers reported that using RuO_2 improved the electrode performance of porous $LiFePO_4$.[33] RuO_2-containing composites reveal reversible capacities of 124 and 93 mA h g^{-1} at rates of 2 C and 10 C, respectively. It is worth noting that quantum dots (QDs) with small size shorten the diffusion length for Li^+, which is beneficial to achieve cycling stability and rate capability. Han *et al.* constructed the V_2O_5 QDs–graphene hybrid nanocomposite exhibiting stable cycling ability and high reversible capacity.[36] Mo *et al.* also synthesized the TiO_2 QDs–graphene nanosheets, which revealed enhanced electrochemical performance.[37]

Herein, to take the advantages of RuO_2, QDs and V_2O_5, we designed and synthesized bowknot-like RuO_2 quantum dots@V_2O_5 (denoted as RQDV) nanomaterials *via* a facile and rapid hydrothermal synthesis method followed by annealing treatment. To our knowledge, the bowknot-like RQDV has not been reported before. As shown in Scheme 1, the RuO_2 QDs exhibit excellent electronic conductivity and fast Li^+ permeation.[34] The RuO_2 QDs dispersed on the bowknot-like V_2O_5

State Key Laboratory of Advanced Technology for Materials Synthesis and Processing, WUT-Harvard Joint Nano Key Laboratory, Wuhan University of Technology, Wuhan, 430070, P. R. China. E-mail: mlq518@whut.edu.cn; Fax: +86-027-87644867; Tel: +86-027-87467595

† Electronic supplementary information (ESI) available: The XRD patterns of the prepared RQDV precursor; the low and high magnification FESEM images of the RQDV precursor, respectively; FESEM images of the RQDV precursor obtained at different hydrothermal time: 30 min, 1 h, 2 h and 6 h; a representative CV curve of an electrode based on the V_2O_5 electrode obtained at a voltage range of 2.0 to 4.0 V (*vs.* Li^+/Li) at scan rate of 0.1 mV s^{-1}; voltage profiles plotted for the 1st, 5th, 50th and 100th cycles of a V_2O_5 electrode at a current density of 100 mA g^{-1}; XRF of the RQDV. See DOI: 10.1039/c4cp02762k

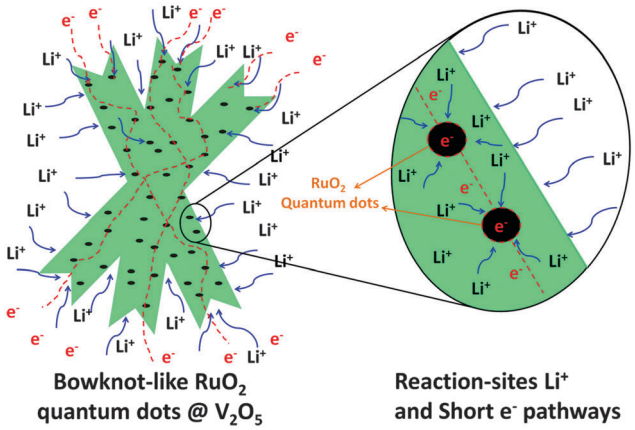

Scheme 1 Schematic illustration of the bowknot-like RuO_2 quantum dots@V_2O_5 with accessible intercalation sites for Li^+ and short electron/ion transport pathways.

enhance the electronic conductivity of this material. The unique nanostructure with RuO_2 QDs dispersing on the V_2O_5 offers reaction sites for Li^+ and short electron transport pathways. The RQDV cathode shows a higher rate capability and better cycling stability than the pure V_2O_5 cathode.

Experimental section

Sample preparation

The RQDV was synthesized as follows: vanadium pentoxide (V_2O_5) powder (1 mmol) dispersed in deionized water (30 mL) and hydrogen peroxide solution (5 mL, 30%) was added under stirring until a clear orange solution formed. After that, ammonium dihydrogen phosphate ($NH_4H_2PO_4$) (1.5 mmol) was added in the solution. Then, 0.8 mL ruthenium chloride solution (0.1 mol L^{-1}) was added to the above solution. Finally, the resulting solution was transferred into a Teflon-lined stainless steel autoclave and kept at 180 °C for 3 h. The products were washed repeatedly with deionized water and ethanol, and finally dried at 70 °C for 12 h. The as-prepared samples were annealed at 450 °C for 3 h at a ramping rate of 3 °C min^{-1}.

The sample prepared by the hydrothermal process followed by annealing with $RuCl_3$ is noted as RQDV. The sample without $RuCl_3$ after annealing is noted as the pure V_2O_5. The sample without annealing is noted as the RQDV precursor.

Material characterization

X-ray diffraction (XRD) measurements were performed to obtain the crystallographic information using a D8 Advance X-ray diffractometer with a non-monochromated Cu Kα X-ray source. Field emission scanning electron microscopic (FESEM) images and energy dispersive spectra (EDS) were collected using a JEOL-7100F microscope. X-ray photoelectron spectroscopy (XPS) analysis was done on a VG Multilab 2000. Transmission electron microscopic (TEM) and high-resolution TEM (HRTEM) images were recorded using a JEOL JEM-2100F STEM/EDS microscope. X-Ray Fluorescence (XRF) analysis was conducted using an Axios advanced X-ray fluorescence spectrometer JY/T 016-1996.

Electrochemical measurements

The electrochemical measurements were carried out by assembly of 2016 coin cells in a glove box filled with pure argon gas, using lithium discs as both the counter electrode and the reference electrode, and 1 M $LiPF_6$ in a mixture of ethylene carbon–dimethyl carbonate (1 : 1 w/w) as the electrolyte. Cathodes were obtained with 70% active material, 20% acetylene black and 10% poly(tetrafluoroethylene) (PTFE). Galvanostatic charge–discharge tests were performed at a potential range of 2.0–4.0 V *vs.* Li^+/Li using a multichannel battery testing system (LAND CT2001A). Cyclic voltammetry (CV) and electrochemical impedance spectra (EIS) were tested using an electrochemical workstation (Autolab PGSTAT 302N).

Results and discussion

Fig. 1a shows the XRD patterns of the pure V_2O_5 and RQDV. The pure V_2O_5 matches well with the orthorhombic V_2O_5 phase (JCPDS card No. 00-001-0359) with no impurity phase. The as-prepared RQDV is well crystallized and exhibits the standard diffraction peaks of the orthorhombic V_2O_5 phase. In addition, the standard diffraction peaks of RuO_2 also exist corresponding to JCPDS card No. 00-050-1428, which reveals that RuO_2 is formed during the synthesis process. The formation of the RuO_2 QDs may be due to the hydrogen peroxide in the solution converting Ru(III) to RuO_2 nanoparticles in the hydrothermal process at 180 °C and subsequent crystallization in the annealing process.[38,39] The XRD pattern of the RQDV precursor (ESI,† Fig. S1) was also measured. The peak intensity of the RQDV precursor is very weak, which indicates that the RQDV precursor has very low crystallinity. Fig. 1b shows the low-magnification FESEM image of the RQDV precursor, which exhibits uniform bowknot-like structure. The high-magnification FESEM image (Fig. 1c) shows that bowknot-like structure is composed of hierarchical assemblies of a single nanosheet with a transverse diameter of 50–200 nm. The EDS analysis of the bowknot-like nanomaterials indicates their chemical composition corresponding well to that of the RQDV (Fig. 1d). Fig. 1e and f present the low- and high-magnification FESEM images of the RQDV, respectively. It can be seen that the bowknot-like structure can be retained well after calcination. The low-magnification FESEM image of the pure V_2O_5 precursor shows that nanobelts extend continuously around a center (ESI,† Fig. S2a). The morphology of this sample can be further observed by the high-magnification FESEM image, which shows the structure of nanoribbons with an average diameter of ~100 nm (ESI,† Fig. S2b). After annealing, some nanobelts were damaged and aggregated (ESI,† Fig. S2c and d).

Time-dependent experiments were conducted to further understand the formation process of bowknot-like structure. The samples were collected at different stages during the synthesis process, and their morphologies were investigated by SEM (ESI,† Fig. S3). When the reaction time was 30 min,

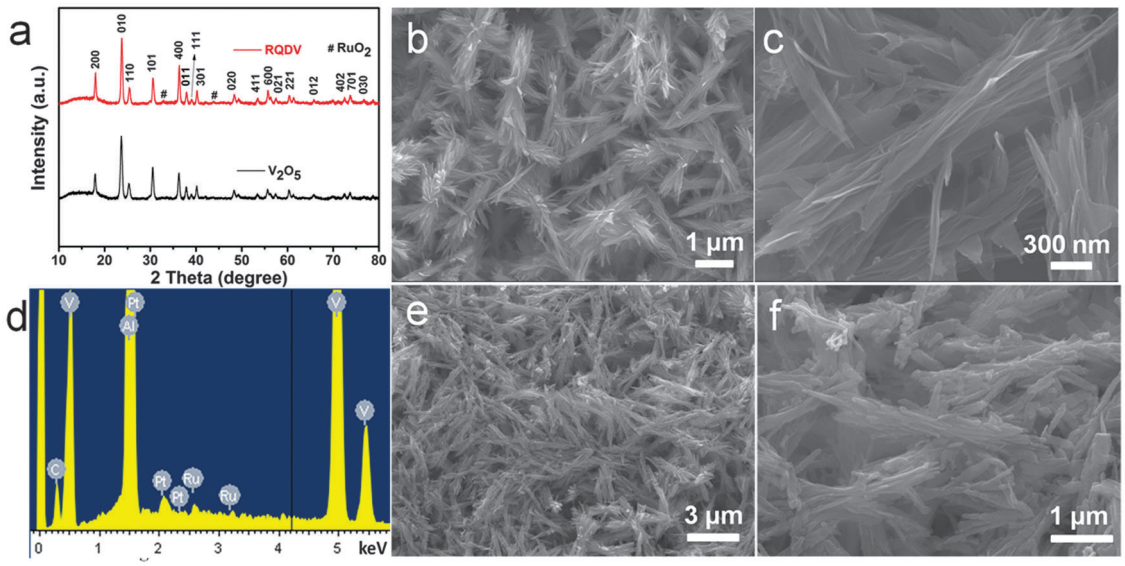

Fig. 1 (a) The XRD patterns of the prepared V_2O_5 and RQDV; (b and c) the low and high magnification FESEM images of the RQDV precursor, respectively. (d) The EDS pattern of RQDV; (e and f) the low- and high-magnification FESEM images of RQDV, respectively.

some nanosheets were formed and aggregated (ESI,† Fig. S3a). As the reaction time increased to 1 h, more nanosheets were formed and constructed into bowknot-like structure (ESI,† Fig. S3b). With the reaction time prolonging to 2 h, some nanoflowers assembled by nanosheets through the Ostwald ripening process can be observed (ESI,† Fig. S3c). As the reaction time increased to 6 h, bowknot-like structure was formed, which was similar to that obtained at the initial stage (ESI,† Fig. S3d).

Fig. 2a shows the low magnification TEM image of the annealed RQDV, which further indicates the high thermal stability of the bowknot-liked structure. The high magnification TEM image of annealed RQDV (Fig. 2b) exhibits nanometer-sized RuO_2 (0.5–3.5 nm) dispersed on the surface of V_2O_5. Fig. 2c shows the high resolution transmission electron microscopy (HRTEM) image of the annealed RQDV. The lattice spacing of 2.61 Å is indexed to the (301) set of planes of the orthorhombic V_2O_5 (JCPDS card No. 00-001-0359); it can be also observed that the lattice spacing of 2.79 Å indexed to the (111) set of planes of the RuO_2 (JCPDS card No. 00-050-1428) exists. The particle size distribution of RuO_2 is obtained through statistically analyzing the HRTEM of the RQDV (Fig. 2d). It exhibits that over 80% of the RuO_2 QDs are in the size range of 1–2.5 nm.

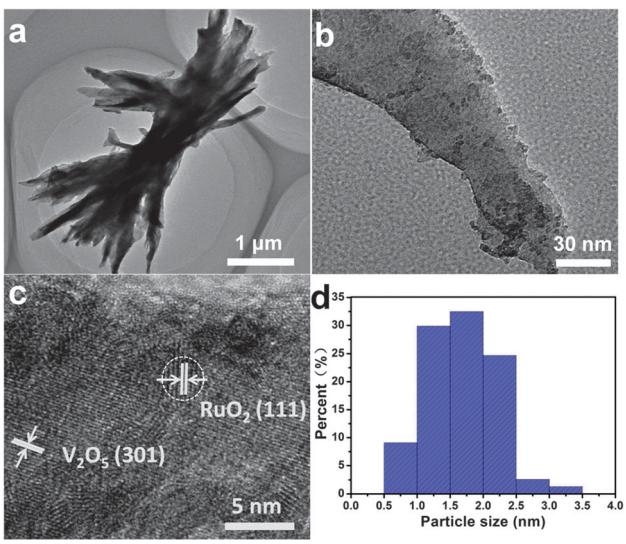

Fig. 2 (a) The low- and (b) high-magnification TEM images and (c) the high-resolution TEM (HRTEM) images of the annealed RQDV, respectively. (d) Particle size distribution of RuO_2 QDs on V_2O_5.

XRF analysis was performed to examine the composition of annealed RQDV. The XRF table shows that the as-obtained samples mainly contain V_2O_5 and RuO_2, which reveals that the mass percentage of RuO_2 is 2.56% in the composite (ESI,† Table S1). XPS measurements were conducted to further confirm the oxidation state of vanadium and ruthenium. Fig. 3a shows the binding energy for V $2p_{3/2}$ at 517.2 eV, which corresponds to V^{5+} in V_2O_5 according to the previous report.[40] Fig. 3b presents the spectra for Ru $3d_{5/2}$ and C 1s. The Ru $3d_{5/2}$ band was observed at 281.0 eV attributed to Ru^{4+} in RuO_2.[41] The C 1s band at 284.6 eV may be from the effect of the atmosphere.[42]

Various electrochemical measurements were performed to contrast the electrochemical performances of the as-prepared samples (Fig. 4). The cyclic voltammetry (CV) curve of the RQDV electrode was tested at a scan rate of 0.1 mV s^{-1} in the potential range from 2.0 to 4.0 V (Fig. 4a). It is clear that three pairs of redox peaks appear at 2.588/2.196, 3.291/3.118 and 3.493/3.323 V, which can be attributed to the Li-ion insertion and extraction processes, corresponding to the phase transitions from α-V_2O_5 to ε-$Li_{0.5}V_2O_5$, ε-$Li_{0.5}V_2O_5$ to δ-LiV_2O_5 and δ-LiV_2O_5 to γ-$Li_2V_2O_5$, respectively (eqn (1)–(3)).[43]

$$V_2O_5 + 0.5Li^+ + 0.5e^- = \varepsilon\text{-}Li_{0.5}V_2O_5 \quad (1)$$

$$\varepsilon\text{-}Li_{0.5}V_2O_5 + 0.5Li^+ + 0.5e^- = \delta\text{-}LiV_2O_5 \quad (2)$$

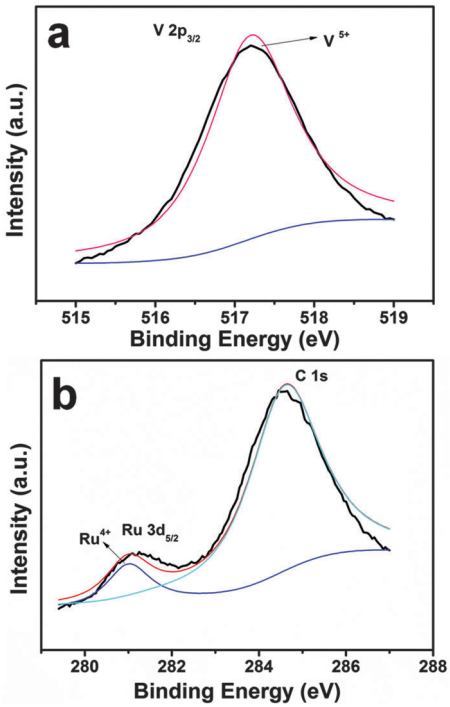

Fig. 3 The XPS spectra for annealed RQDV: (a) the V $2p_{3/2}$ bands; (b) the Ru $3d_{5/2}$ and C 1s bands.

$$\delta\text{-}LiV_2O_5 + Li^+ + e^- = \gamma\text{-}Li_2V_2O_5 \quad (3)$$

The cyclic voltammetry curve of the pure V_2O_5 was also tested at a scan rate of 0.1 mV s^{-1} in the potential range from 2.0 to 4.0 V (ESI,† Fig. S4a). The three main cathodic and anodic peaks correspond to a series of phase transformation. The shape of the pure V_2O_5 is similar to that of the RQDV. However, there are some minor peaks, which may result from structural changes. Fig. 4b shows the charge–discharge voltage profiles for the 1st, 5th, 50th and 100th cycles of RQDV electrode at a current density of 100 mA g^{-1}. There are three voltage plateaus observed in the discharge process, which are in accordance with the redox peaks in CV curves. The charge–discharge voltage profiles for the 1st, 5th, 50th and 100th cycles of the pure V_2O_5 electrode were collected at a current density of 100 mA g^{-1} (ESI,† Fig. S4b). When the cycling numbers reach 50th and 100th cycles, the pure V_2O_5 shows poor reversibility.

Fig. 4c and d show the cycling performances of the pure V_2O_5 and RQDV tested *via* constant current charge–discharge in a voltage range of 2.0–4.0 V cycling up to 100 cycles, which demonstrate the superiority of the RQDV as a cathode material. Fig. 4c shows the comparison of the cycling ability of the pure V_2O_5 and RQDV at a current density of 100 mA g^{-1}. The capacity retentions of the pure V_2O_5 and RQDV after 100 cycles are 62% and 70%, respectively. RQDV reveals better cycling performance delivering relatively high capacity, which may be ascribed to its unique nanostructures with RuO_2 QDs dispersing on the V_2O_5. The cycling performances of the pure V_2O_5 and RQDV electrodes were also tested at a current density of 1 A g^{-1} (Fig. 4d). Compared with RQDV, the pure V_2O_5 delivered a lower capacity of 86 mA h g^{-1} after 100 cycles. The capacity retention of the pure V_2O_5 only remains 65% after 100 cycles, while the capacity retention of RQDV still remains 87%. The RQDV clearly exhibits excellent cycling performance. The capacity retention at 1 A g^{-1} after 100 cycles was much higher than that at 100 mA g^{-1}. Such electrochemical performances may be caused by the following reasons: there are more Li^+ intercalation/de-intercalation in the internal structure of the RQDV electrode at a low current of 100 mA g^{-1}, the structure of the material may be more seriously damaged than that at a high current of 1 A g^{-1} during the charge

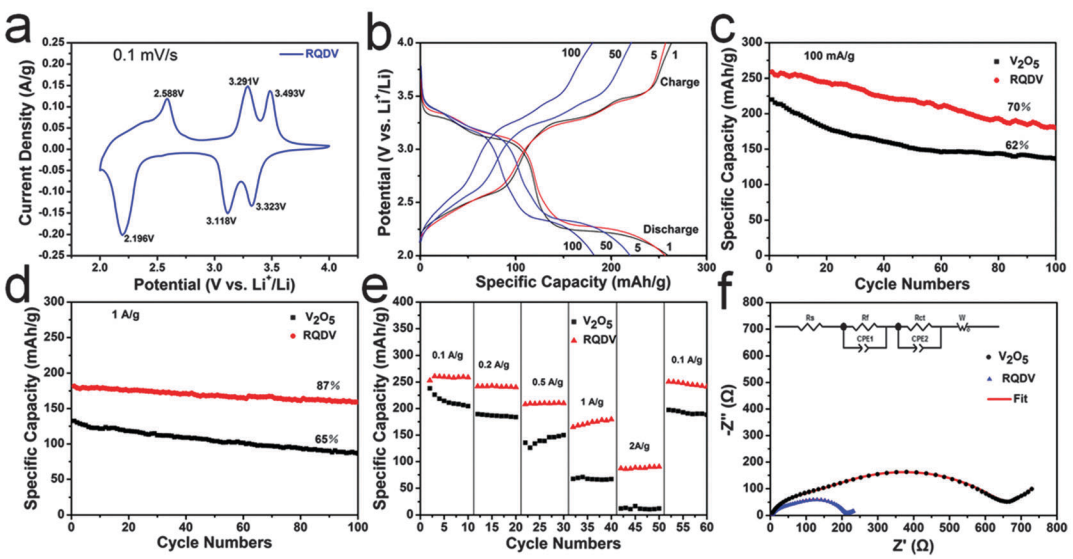

Fig. 4 (a) Representative CV curve of an electrode based on the RQDV electrode obtained at a voltage range of 2.0 to 4.0 V (*vs.* Li^+/Li) at a scan rate of 0.1 mV s^{-1}; (b) voltage profiles plotted for the first, fifth, 50th and 100th cycles of the RQDV composite electrode at a current density of 100 mA g^{-1}. (c, d) The cycling performances of the pure V_2O_5 and RQDV electrodes at current densities of 100 mA g^{-1} and 1 A g^{-1}, respectively; (e) the rate performances of the pure V_2O_5 and RQDV electrodes at different current densities; (f) the Nyquist plots of the pure V_2O_5 and RQDV electrodes.

and discharge process. Similar phenomena are also reported.[44] The rate performances of the pure V_2O_5 and RQDV were studied at different charge/discharge rates from 100 to 2000 mA g^{-1} (Fig. 4e). The RQDV electrode shows 175 and 90 mA h g^{-1}, which is much higher than that of the pure V_2O_5 electrode (88 and 11 mA h g^{-1}) at current densities of 1000 and 2000 mA g^{-1}, respectively. The RQDV exhibits much better electrochemical performance compared with the pure V_2O_5, especially at high current density, which further demonstrates the advantage of the RQDV as LIB cathode materials. Fig. 4f shows the electrochemical impedance spectra of the pure V_2O_5 and RQDV electrodes. The Nyquist plots show that the charge transfer resistance (R_{ct}) of RQDV (139 Ω) is much smaller than that of the pure V_2O_5 (549 Ω), which indicates that the charge transfer kinetics of RQDV is faster than that of the pure V_2O_5.[45,46]

The RQDV cathode exhibits higher rate performance and better cycling stability in comparison with the pure V_2O_5 cathode. The RQDV cathode delivers 160 mA h g^{-1} at a high current density of 1000 mA g^{-1} after 100 cycles, which is much higher than 86 mA h g^{-1} of the pure V_2O_5 cathode. Especially, it still delivers a capacity of 90 mA h g^{-1} at a high current density of 2000 mA g^{-1}, whereas the capacity of the pure V_2O_5 is negligible. The electrochemical performances of RuO_2 QDs@V_2O_5 are also carefully compared with other previous studies (ESI,† Table S2). The RQDV shows good cycling stability and superior rate performance. The impressive electrochemical performances of RQDV can be attributed to the following advantages: (1) the unique RQDV nanostructure offers accessible intercalation sites and shortens Li^+ and e^- transport pathways, which favors electrolyte penetration and interface reactions;[36,47,48] (2) RuO_2 QDs are dispersed on the V_2O_5 surface, which enhances the electronic conductivity of this material. The effect of introducing RuO_2 QDs is remarkable. This point has also been confirmed by other reports.[33,49]

Conclusions

In summary, we have successfully synthesized the bowknot-like RuO_2 quantum dots@V_2O_5 nanomaterials by a facile hydrothermal synthesis method followed by annealing treatment at 450 °C in air. The RuO_2 QDs have a diameter of 0.5–3.5 nm. The electrochemical tests demonstrate that the RQDV cathode exhibits enhanced electrochemical performance. Especially, it delivers a capacity of 160 mA h g^{-1} at a high current density of 1000 mA g^{-1} and improves the cycling stability (87% capacity retention after 100 cycles), whereas the capacity for the pure V_2O_5 is 86 mA h g^{-1} (65% capacity retention after 100 cycles). The enhanced electrochemical performance can be ascribed to the unique nanostructure with RuO_2 QDs dispersed on the V_2O_5 surface. This strategy can be also used as an effective technique for improving the electrochemical performance of other electrodes especially at high rate.

Conflicts of interest

All authors discussed the results and commented on the manuscript. The authors declare no competing financial interest.

Acknowledgements

This work was supported by the National Basic Research Program of China (2013CB934103, 2013DFA50840), the National Natural Science Foundation of China (51272197) and the Fundamental Research Funds for the Central Universities (2013-VII-028, 2014-YB-001, 2014-YB-002).

Notes and references

1 P. Yang and J. M. Tarascon, *Nat. Mater.*, 2012, **11**, 560.
2 B. Kang and G. Ceder, *Nature*, 2009, **458**, 190.
3 M. Armand and J.-M. Tarascon, *Nature*, 2008, **451**, 652.
4 L. Hu, H. Wu, F. L. Mantia, Y. Yang and Y. Cui, *ACS Nano*, 2010, **4**, 5843.
5 N. Mahmood, C. Zhang, H. Yin and Y. Hou, *J. Mater. Chem. A*, 2014, **2**, 15.
6 R. Hu, W. Sun, H. Liu, M. Zeng and M. Zhu, *Nanoscale*, 2013, **5**, 11971.
7 Y. Yao, M. T. McDowell, I. Ryu, H. Wu, N. Liu, L. Hu, W. D. Nix and Y. Cui, *Nano Lett.*, 2011, **11**, 2949.
8 S. Wang, S. Li, Y. Sun, X. Feng and C. Chen, *Energy Environ. Sci.*, 2011, **4**, 2854.
9 M. S. Whittingham, *Chem. Rev.*, 2004, **104**, 4271.
10 V. Raju, J. Rains, C. Gates, W. Luo, X. Wang, W. F. Stickle, G. D. Stucky and X. Ji, *Nano Lett.*, 2014, **14**, 4119.
11 H. Yu, X. Rui, H. Tan, J. Chen, X. Huang, C. Xu, W. Liu, Y. Denis, H. H. Hng and H. E. Hoster, *Nanoscale*, 2013, **5**, 4937.
12 R. Baddour-Hadjean, J. Pereira-Ramos, C. Navone and M. Smirnov, *Chem. Mater.*, 2008, **20**, 1916.
13 L. Mai, F. Dong, X. Xu, Y. Luo, Q. An, Y. Zhao, J. Pan and J. Yang, *Nano Lett.*, 2013, **13**, 740.
14 L. Mai, L. Xu, C. Han, X. Xu, Y. Luo, S. Zhao and Y. Zhao, *Nano Lett.*, 2010, **10**, 4750.
15 J. W. Lee, S. Y. Lim, H. M. Jeong, T. H. Hwang, J. K. Kang and J. W. Choi, *Energy Environ. Sci.*, 2012, **5**, 9889.
16 J. Liu, X. Wang, Q. Peng and Y. Li, *Adv. Mater.*, 2005, **17**, 764.
17 B. Li, Y. Xu, G. Rong, M. Jing and Y. Xie, *Nanotechnology*, 2006, **17**, 2560.
18 Y. Wang, H. J. Zhang, W. X. Lim, J. Y. Lin and C. C. Wong, *J. Mater. Chem.*, 2011, **21**, 2362.
19 V. Mohan, B. Hu, W. Qiu and W. Chen, *J. Appl. Electrochem.*, 2009, **39**, 2001.
20 Q. An, Q. Wei, L. Mai, J. Fei, X. Xu, Y. Zhao, M. Yan, P. Zhang and S. Huang, *Phys. Chem. Chem. Phys.*, 2013, **15**, 16828.
21 Y. Wang and G. Cao, *Adv. Mater.*, 2008, **20**, 2251.
22 A. M. Cao, J. S. Hu, H. P. Liang and L. J. Wan, *Angew. Chem., Int. Ed.*, 2005, **44**, 4391.
23 D. Yu, C. Chen, S. Xie, Y. Liu, K. Park, X. Zhou, Q. Zhang, J. Li and G. Cao, *Energy Environ. Sci.*, 2011, **4**, 858.
24 Q. Shi, J. Liu, R. Hu, M. Zeng, M. Dai and M. Zhu, *RSC Adv.*, 2012, **2**, 7273.
25 M. G. Kim and J. Cho, *Adv. Funct. Mater.*, 2009, **19**, 1497.
26 Q. Shi, R. Hu, L. Ouyang, M. Zeng and M. Zhu, *Electrochem. Commun.*, 2009, **11**, 2169.

27 Y. Wei, C. W. Ryu and K. B. Kim, *J. Power Sources*, 2007, **165**, 386.
28 F. S. Gittleson, J. Hwang, R. C. Sekol and A. D. Taylor, *J. Mater. Chem. A*, 2013, **1**, 7979.
29 Z. Li and E. Ruckenstein, *Langmuir*, 2002, **18**, 6956.
30 L. Xu, Y. Liu, M. P. Garrett, B. Chen and B. Hu, *J. Phys. Chem. C*, 2013, **117**, 10264.
31 X. Chen, H. Zhu, Y.-C. Chen, Y. Shang, A. Cao, L. Hu and G. W. Rubloff, *ACS Nano*, 2012, **6**, 7948.
32 X. F. Zhang, K. X. Wang, X. Wei and J.-S. Chen, *Chem. Mater.*, 2011, **23**, 5290.
33 Y. S. Hu, Y. G. Guo, R. Dominko, M. Gaberscek, J. Jamnik and J. Maier, *Adv. Mater.*, 2007, **19**, 1963.
34 P. Balaya, H. Li, L. Kienle and J. Maier, *Adv. Funct. Mater.*, 2003, **13**, 621.
35 E. Bekaert, P. Balaya, S. Murugavel, J. Maier and M. Ménétrier, *Chem. Mater.*, 2009, **21**, 856.
36 C. Han, M. Yan, L. Mai, X. Tian, L. Xu, X. Xu, Q. An, Y. Zhao, X. Ma and J. Xie, *Nano Energy*, 2013, **2**, 916.
37 R. Mo, Z. Lei, K. Sun and D. Rooney, *Adv. Mater.*, 2014, **26**, 2084.
38 H. Wang, Y. Liang, T. Mirfakhrai, Z. Chen, H. S. Casalongue and H. Dai, *Nano Res.*, 2011, **4**, 729.
39 H. Yu, K. Zeng, X. Fu, Y. Zhang, F. Peng, H. Wang and J. Yang, *J. Phys. Chem. C*, 2008, **112**, 11875.
40 M. Sathiya, A. Prakash, K. Ramesha, J. M. Tarascon and A. Shukla, *J. Am. Chem. Soc.*, 2011, **133**, 16291.
41 C. S. Huang, M. Houalla, D. M. Hercules, C. L. Kibby and L. Petrakis, *J. Phys. Chem.*, 1989, **93**, 4540.
42 C. Yang, G. Wang, Z. Lu, J. Sun, J. Zhuang and W. Yang, *J. Mater. Chem.*, 2005, **15**, 4252.
43 A. Pan, J. G. Zhang, Z. Nie, G. Cao, B. W. Arey, G. Li, S. Q. Liang and J. Liu, *J. Mater. Chem.*, 2010, **20**, 9193.
44 R. Yu, C. Zhang, Q. Meng, Z. Chen, H. Liu and Z. Guo, *ACS Appl. Mater. Interfaces*, 2013, **5**, 12394.
45 Q. Wei, Q. An, D. Chen, L. Mai, S. Chen, Y. Zhao, M. H. Kalele, L. Xu, A. M. Khan and Q. Zhang, *Nano Lett.*, 2014, **14**, 1042.
46 L. Shen, H. Li, E. Uchaker, X. Zhang and G. Cao, *Nano Lett.*, 2012, **12**, 5673.
47 J. G. Kang, J. G. Park and D. W. Kim, *Electrochem. Commun.*, 2010, **12**, 307.
48 F. Croce, A. D Epifanio, P. Reale, L. Settimi and B. Scrosati, *J. Electrochem. Soc.*, 2003, **150**, A576.
49 F. Zhang, S. Passerini, B. B. Owens and W. H. Smyrl, *Electrochem. Solid-State Lett.*, 2001, **4**, A221.